Available online at www.sciencedirect.com
SCIENCE DIRECT®
Earth and Planetary Science Letters 248 (2006) 132–137
EPSL
www.elsevier.com/locate/epsl

An *ab initio* study of nickel substitution into iron

Lidunka Vočadlo *, David P. Dobson, Ian G. Wood

Department of Earth Sciences, UCL, Gower Street, London, WC1E 6BT, UK

Received 21 March 2006; received in revised form 16 May 2006; accepted 20 May 2006
Available online 11 July 2006
Editor: G.D. Price

Abstract

Ab initio calculations at 0 K have been used to predict the effect of nickel on the phase stability of the body-centred-cubic (bcc), face-centred-cubic (fcc) and hexagonal-close-packed (hcp) phases of iron. We have calculated the relative stability of hcp-Fe in the ferromagnetic and two antiferromagnetic structures (afmI and afmII) and find the afmII structure to be the more stable at low pressures (below 50 GPa), in agreement with previous work. We also find our calculated equations of state for pure iron to be in excellent agreement with previous calculations. Small amounts of nickel (3.5 atm.% and 7 atm.%) were then substituted into each phase to see the effect on the equations of state and the bcc–hcp transition pressure. Our results show that the addition of nickel stabilises the hcp structure with respect to bcc by up to ~20 GPa.

Keywords: iron–nickel alloy; *ab initio* simulation; Earth's inner core; phase stability

1. Introduction

Determining the crystal structure of the inner-core phase of the Earth is vital for understanding inner-core seismic anisotropy and evolution. The Earth's core has long been considered to consist of iron–nickel alloy plus a few percent of light alloying elements [1]. The nature of the light component, however, is still a matter of considerable debate despite several decades of work in this area. Attempts to constrain the light element composition of the core fall into two broad categories: (i) estimates of the missing light element inventory of the silicate Earth compared with primitive meteorite composition (e.g.; [2]) and (ii) comparison of observed physical properties of the core (such as radially averaged seismic velocities) with experimental and theoretical estimates of those properties for Fe-alloys under the pressure and temperature conditions of the core. These latter estimates have so far neglected the effect of nickel, as this is considered to be relatively minor compared to light element effects, concentrating instead on Fe-light element binary or ternary systems. Here we present the first *ab initio* study of the effect of nickel on (i) the low-pressure bcc–hcp phase stability in iron, and (ii) the equations of state of iron, for Fe–Ni alloys with compositions relevant to the Earth's core.

At ambient conditions, iron crystallises in the body-centred-cubic (bcc) structure, with face-centred-cubic (fcc) iron stable at temperatures above 1183 K (at 1 atm) and hexagonal-close-packed (hcp) iron stable above ~15 GPa (at room temperature). Recent studies

* Corresponding author.
E-mail address: l.vocadlo@ucl.ac.uk (L. Vočadlo).

0012-821X/$ - see front matter © 2006 Elsevier B.V. All rights reserved.
doi:10.1016/j.epsl.2006.05.028

(e.g. [3]) suggest that, at the pressures and temperatures of the inner core, the free energies of bcc- and hcp-structured pure iron are almost identical, marginally favouring hcp-iron. However, two of the major candidates for the light element, Si and S, have been found to crystallise at high pressures with the CsCl structure (which has atoms in identical positions to the bcc structure) [4–6] which suggests that they might stabilise a bcc phase at core conditions. Further evidence for this supposition comes from the work of Lin et al. [7], where it was shown that the addition of ~8 wt.% silicon to iron extends the stability field of the bcc structure to pressures well above ~15 GPa, the transition pressure to the hcp phase for pure iron. Nickel, by contrast, crystallises in the fcc structure and stabilises fcc Fe–Ni alloys relative to pure Fe (e.g.; [8–11]); both Lin et al. [10] and Mao et al. [11] have found regions of fcc and hcp phase coexistence at high pressures and temperatures.

2. Simulations

Fully relaxed, spin-polarised calculations were carried out using the VASP code [12] which is based on density functional theory [13] within the generalised gradient approximation [14]. They were performed using the projected–augmented wave method [15] to calculate the total energy of the system. When using VASP, as the structure relaxes, the ground state ($T=0$) is calculated exactly for each set of ionic positions and the electronic free energy is taken as the quantity to be minimised. Supercells were constructed in the bcc, hcp and fcc structures of iron. In the hcp case, the ferromagnetic (fm) and two antiferromagnetic structures, afmI and afmII [16–19], were tested (see Fig. 1). Nickel was incorporated into the supercells as substitutional defects evenly distributed throughout each structure; the amount of Ni included (0, ~3.5 and ~7 atm.% Ni) bracketed the concentrations likely to exist in the inner core. In practice, this meant for 3.5% Ni, one atom of Ni per 26 atoms Fe in the bcc and fcc structures (27 atom supercell of the primitive bcc and fcc unit cells), two atoms of Ni per 52 atoms of Fe in the hcp fm and afmI structures (54 atom supercell), and two atoms of Ni per 62 atoms in the afmII structure (64 atom supercell). For the ~7% Ni case, the same supercells were used with two atoms of Ni per 25 atoms Fe in the bcc and fcc structures, four atoms of Ni per 50 atoms of Fe in the hcp fm and afmI structures, and four atoms of Ni per 60 atoms in the afmII structure. Where there was more than one Ni defect, the Ni atoms were placed as far away from each other as possible, taking into account the periodic boundary conditions. Initially all atoms were given, as appropriate, non-directional magnetic moments of $\pm 2\ \mu_B$; these moments were then allowed to vary freely for every atom during the calculations. For all pure Fe phases, the magnitude of the moment on each atom remained identical, diminishing with pressure; for the Fe–Ni alloys, the moments on the nickel atoms were much less than those on the iron atoms with the latter showing some variation from atom to atom (e.g. typically less than $\pm 0.3\ \mu_B$ for 7 atm.% Ni). In the case of the afmII structure with ~7 atm.% nickel the supercell allows several choices for the positions of the Ni atoms, either with the same magnetisation sign or oppositely magnetised. Trial calculations showed there to be a negligible difference in energy between different configurations (<1 meV per atom) so the results discussed below refer only to supercells with the former configuration. The presence of nickel locally influences the magnetisation of the iron atoms, those with two nearest neighbour Ni atoms in their close-packed plane being most greatly affected. The k-point sampling grid and plane-wave cut-offs were chosen to give energy convergence to less than 0.005 eV/atom. To achieve this, the k-space integrations were performed using a $5\times5\times5$ Monkhorst–Pack grid [20] for the bcc and fcc phases, and a

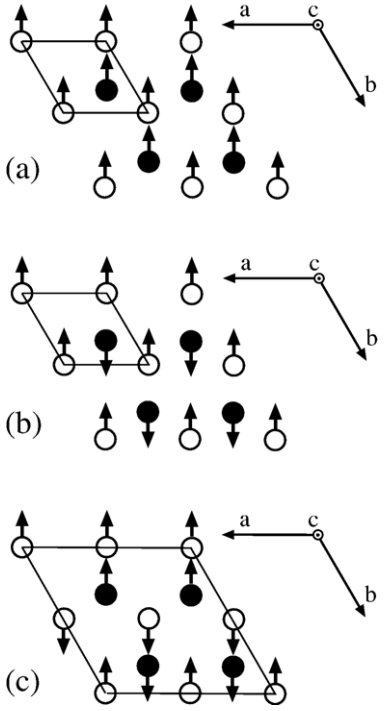

Fig. 1. The magnetic structures of a) fm–hcp-Fe, b) afmI–hcp-Fe, and c) afmII–hcp-Fe, projected along the c axis. The unit cells from which the supercells were constructed for each calculation are indicated by the solid lines (supercells used were: fm — $3\times3\times3$; afmI — $3\times3\times3$; afmII — $2\times2\times2$). Open symbols represent atoms at $z=0$; solid symbols represent atoms at $z=0.5$. Arrows denote the spin state of the atoms, i.e. positive or negative; no directionality is implied.

Table 1
Birch–Murnaghan 3rd order EOS parameters

Atm.% Ni	Fe structure	V_0 (Å^3)	[$K'=4$]	K_0 (GPa)	[$K'=4$]	K'	[$K'=4$]	E_0 (eV)	[$K'=4$]
0	bcc	11.355(7)	[11.23]	201.502(8)	[237]	4.29(1)	[4]	−8.3149(7)	[−8.2002]
	Ref. [21]	11.39		189		4.9			
	fcc	10.37(3)	[10.31]	278.50(7)	[315]	4.5(2)	[4]	−8.0685(75)	[−8.0837]
	Ref. [21]	10.27		288		4.4			
	hcp–fm	10.199(7)	[10.13]	293.05(2)	[327]	4.36(3)	[4]	−8.2655(9)	[−8.2692]
	Ref. [21]	10.20		291		4.4			
	hcp–afmI	10.205(8)		291.43(2)		4.38(3)		−8.2659(9)	
	Ref. [16]	10.45		210		5.5			
	hcp–afmII	10.43(2)	[10.32]	237.80(4)	[297]	4.8(1)	[4]	−8.2875(29)	[−8.3048]
	Ref. [16]	10.55		209		5.2			
	Ref. [18]	10.43		213		6.1			
	Ref. [17]	10.43		210		6.2			
~3.5	bcc	11.49(3)	[11.32]	184.74(3)	[223]	4.53(7)	[4]	−8.0998(18)	[−8.0996]
	fcc	10.298(6)	[10.18]	293.07(1)	[335]	4.36(1)	[4]	−7.9590(7)	[−7.9538]
	hcp–fm	10.164(9)	[10.10]	309.79(2)	[333]	4.18(2)	[4]	−8.1437(12)	[−8.1375]
	hcp–afmI	10.184(9)		304.01(2)		4.22(3)		−8.1505(11)	
	hcp–afmII	10.29(3)	[10.23]	277.00(5)	[304]	4.42(8)	[4]	−8.1802(22)	[−8.1800]
~7	bcc	11.57(6)	[11.32]	170.48(5)	[222]	4.64(11)	[4]	−7.9935(37)	[−7.9917]
	fcc	10.34(2)	[10.17]	283.65(3)	[337]	4.42(4)	[4]	−7.8614(25)	[−7.8437]
	hcp–fm	10.215(6)	[10.16]	298.88(1)	[323]	4.24(2)	[4]	−8.0284(9)	[−8.0306]
	hcp–afmI	10.20(1)		303.87(3)		4.21(3)		−8.1152(18)	
	hcp–afmII	10.35(2)	[10.26]	240.76(5)	[295]	4.8(1)	[4]	−8.1288(42)	[−8.1487]

For each structure and composition, the fitted values of V_0, K_0, K' and E_0 (per atom) are listed, with their estimated standard errors in parentheses; the corresponding parameters with K' fixed at 4 are also shown in square brackets.

$2\times2\times2$ grid for the hcp phase; the plane-wave basis set cut-off energy was 400 eV. The procedure adopted to determine the equations of state was to use VASP to calculate the internal energy (E) of the crystal at a set of chosen volumes (V). The resulting E–V data were then fitted to an integrated 3rd-order Birch–Murnaghan equation-of-state (EOS) (see, e.g., [4] for details). The resulting EOS parameters were subsequently used to obtain P–V relations and the relative stabilities of the pure and nickel substituted phases were then obtained by inspection of their enthalpy–volume curves.

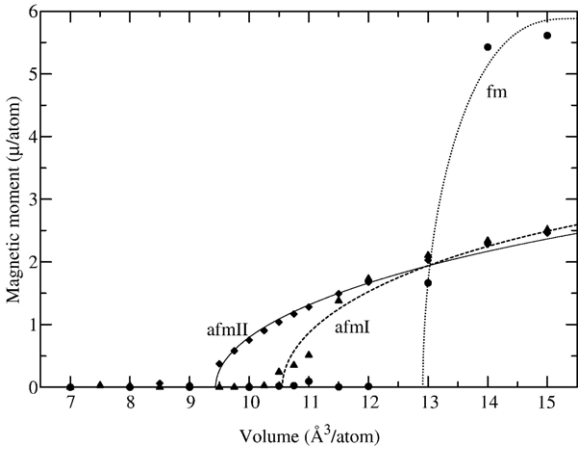

Fig. 2. The magnetic moment per atom of ferromagnetic, afmI and afmII–hcp-Fe as a function of volume. For $P>0$ ($V<10.2$ Å^3) neither hcp–fm nor hcp–afmI retain a magnetic moment on the atoms; in the afmII structure the magnetic moment persists to moderate pressures (~50 GPa). The lines shown are mean-field magnetization curves fitted to the calculated points and serve as guides to the eye.

3. Results

Table 1 shows the equation-of-state parameters for each of the pure iron and Fe–Ni alloy systems. At first sight, on inspection of Table 1, it would appear that adding small amounts of nickel to iron does not seem to noticeably change the EOS parameters for any of the structures modelled. For all compositions, the EOS of the fm–hcp and afmI–hcp phases are almost identical; this is not surprising as both phases have a magnetic moment per atom that is non-zero only at negative pressures (Fig. 2). There is a greater difference with composition between the EOS parameters for the afmII–hcp structures; the magnetic moment per atom of the afmII–hcp phase persists to ~50 GPa, this phase being the stable hcp phase at low pressures (Fig. 3) as also predicted by earlier calculations [16–19]. However, if the EOS parameters from Table 1 are used to obtain enthalpy–pressure relationships to determine the relative stability of each phase, a

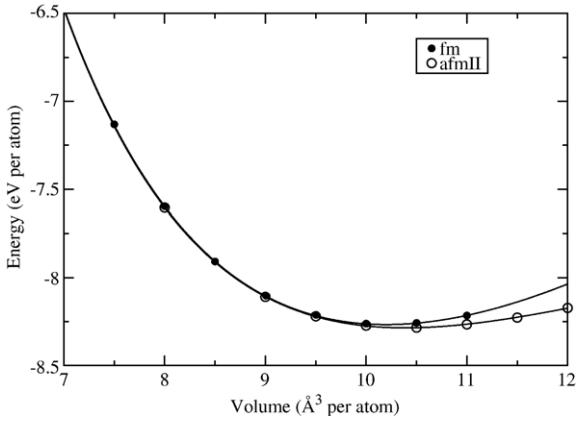

Fig. 3. Energy as a function of volume for pure hcp-Fe in the fm and afmII structures. The afmII structure is more stable at low pressures; the energies converge at higher pressures when the magnetic moment is lost.

systematic trend with nickel content is revealed. For all compositions, the afmII phase of the hcp structures is the most stable; we therefore do not consider further the hcp–fm and hcp–afmI structures.

Fig. 4 shows how the enthalpy varies as a function of pressure for the bcc, fcc and hcp–afmII phases for the three Fe–Ni compositions. In all cases, the fcc structure is the least stable (we note that, although our calculation for the fcc phase neglects the complex spin-wave structure, the maximum energy difference between the simple fcc ferromagnetic phase and fcc structures with different spin-wave vectors is ~0.08 eV [22], significantly smaller than the energy difference (>0.25 eV) between the fcc phase and the other phases shown in Fig. 4).

Also, for all compositions shown in Fig. 4, a transition from the bcc structure to the hcp–afmII structure is observed, although this transition occurs at negative pressure for the iron–nickel compositions modelled. It is clear, therefore, that the presence of nickel stabilises the hcp phase with respect to bcc at low pressures; the pressures at which the bcc to hcp–afmII transition occurs are approximately 6 GPa. −11 GPa and −18 GPa for concentrations of nickel of 0 atm.%, 3.5 atm.% and 7 atm.% respectively. The effect of nickel on the fcc phase is also to stabilise it with respect to the bcc phase, with transition pressures for 0 atm.%, 3.5 atm.% and 7 atm.% Ni of 61 GPa, 26 GPa, 22 GPa respectively (not shown in Fig. 4). However, at no pressure is the fcc structure the most stable; in all cases the hcp phase remains the stable phase to core pressures. These results are consistent with the experimentally observed depression of the bcc–hcp transition pressure [23] and the stabilisation of the fcc over the bcc structure in Fe–Ni at 1 atm [24]. We note that for at least some of the compositions studied here the phases can exist only metastably at low pressure [24]. However, the present study aims to explore tendencies rather than to provide full thermodynamic equilibrium calculations.

Precise determination of the variation with composition of the pressure at which the bcc to hcp–afmII transition occurs is hampered by the near parallel nature of the enthalpy curves. From the results shown in Fig. 4, the transition pressure is found to reduce by 3.4(8) GPa

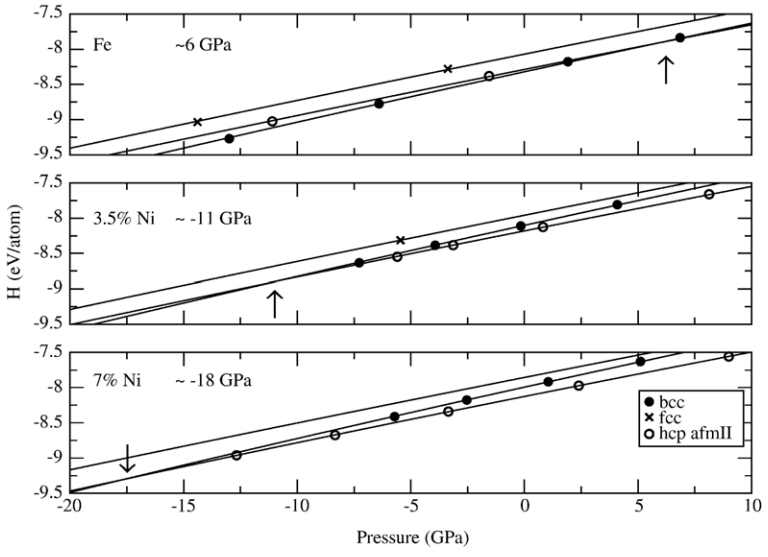

Fig. 4. Enthalpy as a function of pressure for bcc, fcc and hcp–afmII phases with a) 0% nickel, b) ~3.5 atm.% nickel and c) ~7 atm.% nickel. Arrows indicate the transition pressures.

per atm.% Ni. Strictly it is necessary to correct for the slight difference in % Ni due to the different sized supercells used in the calculations. This can be done by using the EOS to construct a set of enthalpy–composition curves for a set of isobars; however, this was found to have a negligible effect, changing the transition pressure gradient by less than one standard error.

4. Discussion and conclusion

This study was motivated by a surprising dearth of information in the literature (even at 0 K) about the effect of nickel on iron phase stability, although we note that a further experimental study has been published very recently by Mao et al. [11]. For pure iron, our results confirm the findings of others [16–19] that the afmII structure is the most stable hcp phase at low pressures. Magnetic structure is irrelevant at core pressures, as above ~50 GPa the magnetic moment disappears, but since the bcc–hcp phase transition occurs below 50 GPa (experimentally determined to be at ~10–15 GPa), magnetism is important in studying this transition. In the past, the transition between bcc and hcp iron has been modelled using the ferromagnetic structure of hcp-Fe, which, both in this study and previously, has led to a calculated transition pressure of ~10 GPa (see e.g., [25]) in approximate agreement with the experimental value. Our calculated transition pressure in the present work between bcc and the hcp–afmII phase for pure iron is a little lower (~6 GPa), reflecting the greater stability of the hcp–afmII structure. When nickel is introduced into the system, it is clear that the hcp–afmII phase is stabilised with respect to the bcc phase at low pressure (and 0 K) by up to 20 GPa. While we recognise that our calculations are athermal and we cannot, therefore, make any assumptions about what will occur at high temperatures, our results do suggest that nickel and light elements such as silicon (which favours bcc) are in direct competition in determining the high P/T structural stability of iron. Clearly, a full free energy calculation at high pressures and temperatures is needed to resolve the matter. However, this initial study is sufficient to suggest that the previously held assumption that nickel has little or no effect on the first-order elastic properties of iron is not necessarily valid.

Acknowledgements

DPD and LV are grateful to the Royal Society for their University Research Fellowships. We thank A. Jackson for the stimulating discussions leading to this study.

References

[1] F. Birch, Elasticity and constitution of the Earth's interior, J. Geophys. Res. 57 (1952) 227–286.
[2] C.J. Allegre, J.-P. Poirier, E. Hummler, A.W. Hofmann, The chemical composition of the Earth, Earth Planet. Sci. Lett. 134 (1995) 515–526.
[3] L. Vočadlo, D. Alfe, M.J. Gillan, I.G. Wood, J.P. Brodholt, G.D. Price, Possible thermal and chemical stabilization of body centred-cubic iron in the Earth's core, Nature 424 (2003) 536–539.
[4] L. Vočadlo, I.G. Wood, G.D. Price, Crystal structure, compressibility and possible phase transitions in epsilon-FeSi studied by first-principles pseudopotential calculations, Acta Crystallogr., B Struct. Sci. 55 (1999) 484–493.
[5] D.P. Dobson, L. Vočadlo, I.G. Wood, A new high-pressure phase of FeSi, Am. Mineral. 87 (2002) 784–787.
[6] P. Martin, G.D. Price, L. Vočadlo, An ab initio study of the relative stabilities and equations of state of FeS polymorphs, Min. Mag. 65 (2001) 181–191.
[7] J.-F. Lin, D.L. Heinz, A.J. Campbell, J.M. Devine, G.Y. Shen, Iron–silicon alloy in the Earth's core? Science 295 (2002) 313–315.
[8] E. Huang, W.A. Bassett, M.S. Weathers, Phase relationships in Fe–Ni alloys at high pressure and temperatures, J. Geophys. Res. 93 (1988) 7741–7746.
[9] E. Huang, W.A. Bassett, M.S. Weathers, Phase diagram and elastic properties of Fe30% Ni alloy by synchrotron radiation, J. Geophys. Res. 97 (1992) 4497–4502.
[10] J.-F. Lin, D.L. Heinz, A.J. Campbell, J.M. Devine, W.L. Mao, G.Y. Shen, Iron–nickel alloy in the Earth's core, Geophys. Res. Lett. 29 (2002) (art. no. 1471).
[11] W. Mao, A.J. Campbell, D.L. Heinz, G. Shen, Phase relations of Fe–Ni alloys at high pressure and temperature, Earth Planet. Sci. Lett. 155 (2006) 146–151.
[12] G. Kresse, J. Furthmüller, Efficient iterative schemes for *ab initio* total-energy calculations using a plane-wave basis set, Phys. Rev., B 54 (1996) 11169–11186.
[13] P. Hohenberg, W. Kohn, Inhomogeneous electron gas, Phys. Rev. 136 (1964) B864–B871.
[14] Y. Wang, J. Perdew, Correlation hole of the spin-polarized electron gas, with exact small-wave-vector and high-density scaling, Phys. Rev., B 44 (1991) 13298–13307.
[15] P.E. Blöchl, Projector augmented-wave method, Phys. Rev., B 50 (1994) 17953–17979.
[16] G. Steinle-Neumann, L. Stixrude, R.E. Cohen, First-principles elastic constants for hcp transition metals Fe, Co and Re at high pressure, Phys. Rev., B 60 (1999) 791–799.
[17] R.E. Cohen, S. Mukherjee, Non-collinear magnetism in iron at high pressures, Phys. Earth Planet. Int. 143–144 (2004) 445–453.
[18] G. Steinle-Neumann, R.E. Cohen, L. Stixrude, Magnetism in iron as a function of pressure, J. Phys., Condens. Matter 16 (2004) S1109–S1119.
[19] G. Steinle-Neumann, L. Stixrude, R.E. Cohen, Magnetism in dense hexagonal iron, Proc. Natl. Acad. Sci. 101 (2004) 33–36.
[20] H.J. Monkhorst, J.D. Pack, Special points for Brillouin zone integrations, Phys. Rev., B 13 (1976) 5188–5192.

[21] L. Stixrude, R.E. Cohen, D.J. Singh, Iron at high pressure — linearised–augmented–planewave computations in the generalized–gradient–approximation, Phys. Rev., B 50 (1994) 6442–6445.
[22] O.N. Mryasov, A.I. Liechtenstein, L.M. Sandratskii, V.A. Gubanov, Magnetic structure of FCC iron, J. Phys., Condens. Matter 3 (1991) 7683–7690.
[23] A. Christou, Stability of magnetic phase-transition in shocked Fe–Ni alloys, Philos. Mag. 27 (1973) 833–852.
[24] E.A. Brandes, G.B. Brook (Eds.), Smithells Metals Reference Book, 7th Edition, Pub. Butterworth–Heinemann Ltd., Oxford, 1992, pp. 11–262.
[25] L.Vočadlo, G. de Wijs, G. Kresse, M.J. Gillan, G.D. Price, First Principles Calculations on Crystalline and Liquid Iron at Earth's Core Conditions. Faraday Discussions 106 'Solid-State Chemistry — New Opportunities from Computer Simulations' (1997) 205–217.